Grazing Incidence Neutron Spin Echo Study of Poly(*N*-isopropylacrylamide) Brushes[†]

Judith Witte,[*,‡] Patrick Krause,[‡] Tetyana Kyrey,[‡,¶] Anna Margarethe Dahl,[‡] Jana Lutzki,[‡] Bernhard V. K. J. Schmidt,[§] Marina Ganeva,[¶] Alexandros Koutsioubas,[¶] Olaf Holderer,[¶] and Stefan Wellert[‡]

‡*Department of Chemistry, Technische Universität Berlin, Berlin, Germany*

¶*JCNS at Heinz Maier-Leibnitz Zentrum, Garching, Germany*

§*Max Planck Institute of Colloids and Interfaces, Potsdam, Germany*

E-mail: judith.witte@tu-berlin.de

Phone: +49 30 314 26774

Abstract

The structure and the dynamic properties of poly(*N*-isopropylacrylamide) brushes at solid planar surfaces under good solvent conditions are studied. Polymer brushes with grafting densities in the high density and semidilute regime are prepared via surface-initiated atom transfer radical polymerization. The polymer brushes were removed from the substrates to determine the molar mass and molecular dispersity via size exclusion chromatography to draw conclusions about the grafting density. The structure of the brushes was investigated with ellipsometry and neutron reflectometry measurements. We find an influence of the grafting density on the swelling properties of the poly(*N*-isopropylacrylamide) brushes. Furthermore, the brush dynamics at different neutron

[†]A footnote for the title

penetration depths was analyzed with neutron spin echo spectroscopy under grazing incidence. The evanescent intensity distribution was modeled with the BornAgain software package, which uses the Distorted Wave Born Approximation.

Introduction

Polymer brushes are polymer chains, end-tethered to a surface with a density of anchor points above a critical overlap density $\sigma^* \cong 1/R_g^2$, where R_g is the radius of gyration in solution under good solvent conditions. Due to the close proximity of neighboring chains a free-energy balance argument between the desire to achieve a random walk configuration to maximize the systems' entropy and the avoidance of polymer-polymer interactions occurs, leading to the stretching away of the polymer chains from the surface resulting in a certain brush height h.[1]

These systems are commonly used for colloidal stabilization and surface modification to enhance certain surface properties such as wettability, antifouling behavior and tribological properties. Taking into consideration the extensive work done in this field, we recommend review articles for orientation.[2–4]

This paper, using the example of poly(N-isopropylacrylamide) (PNIPAM) brushes in a good solvent, explores experimentally the relation between structural features of such polymer brushes and their dynamics. This has mostly been done with neutron spin echo spectroscopy in transmission mode on spherical polymer brushes resulting from micelle like aggregation of A-B diblock copolymers.[5] Furthermore, dynamic light scattering experiments at interfaces employing the occurrence of evanescent waves under total internal reflection (EWDLS) were conducted to investigate the dynamics of flat polymer brushes.[6,7] Such EWDLS measurements probe the thermally excited density fluctuations inside a brush in thermal equilibrium. Beside this, atomic force microscopy (AFM)[8] and surface force measurements (SFA)[9] have been used to explore the relaxations in polymer brushes. This was done either in thermal equilibrium[10,11] or under the influence of an external force.[8] This allows to draw conclusions about the breathing mode of the brush, the adhesive properties and the friction in the brushes.[8–11] However, in this work we aim at grazing incidence neutron spin echo (GINSES) studies of polymer brushes grafted from flat silicon surfaces. These experiments are rather challenging, but in this paper we show how combined with techniques such as ellipsometry

and neutron reflectometry (NR) they help in gaining valuable insights into polymer brush dynamics. Furthermore, the grazing incidence geometry, in contrast to the transmission geometry, allows a unique z-resolution to probe the brush layer in close proximity to the grafting plane and the brush volume towards the bulk phase.[12,13] PNIPAM was chosen since it is a prominent model system used in many polymer systems such as polymer brushes, microgel particles and hydrogels. Oftentimes, the thermoresponsive properties of PNIPAM with a volume phase transition temperature (VPTT) of approximately 32 °C are mentioned and characterized in publications. However, for the sake of our dynamics studies we focused on the swollen brush below the VPTT.

For homodisperse brushes with large brush heights and low grafting densities a parabolic polymer volume fraction profile according to eq 1 is expected as described by self-consistent field (SCF) theory.[14]

$$\Phi(z) = \Phi(0)[1 - (z/h)^2] \tag{1}$$

with z being the distance from the grafting plane, h the height of the polymer brush and $\Phi(0)$ the polymer volume fraction at $z = 0$.

However, for experimentalists the "grafting from" approach commonly used for the preparation of polymer brushes will yield systems with a molecular dispersity above 1. De Vos et al. argue that the scaling behavior is not affected by this fact. It was shown in simulation studies that the polymer volume fraction profile transitions from convex to linear to completely concave with increasing molecular dispersity.[15]
In contrast, the "grafting to" approach while yielding more homodisperse brushes leads to lower grafting densities due to an excluded volume barrier.[16]

Considering the blob picture of polymer brushes, where a blob is describing a chain

segment exhibiting the behavior of a single unperturbed chain,[17] this makes necessary the introduction of the local correlation length (blob size) $\xi(z)$

$$\xi(z) = d\left(\frac{\phi(z)}{\phi(0)}\right)^{\nu/(1-3\nu)} \tag{2}$$

where d describes the average separation between polymer chains ($d \propto 1/\sqrt{\sigma}$) and ν the swelling exponent. For a real chain ν equals 0.588. Therefore, the local monomer concentration *c(z)*, local correlation length ξ(z) and the local elastic modulus $E(z) \approx k_B T/\xi^3(z)$ all depend on the distance to the grafting surface. This is contrary to the simple Alexander - de Gennes model of polymer brushes with its close packed array of uniformly sized blobs.

Simulations of the size of the last blob, where concentration fluctuations are becoming relevant, were carried out and show a relation between the size of the last blob d_{fl} and the entire brush height h of

$$\frac{d_{fl}}{h} \cong 0.286(\sigma R_g^2)^{-\beta} \tag{3}$$

where σ is the grafting density describing the number of chains per surface area. The exponent $\beta = 1/2$ was extracted from the numerical simulations. The local correlation length in relation to the position within the brush is schematically displayed in Figure 1. As was described in simulation studies the size of the last blob d_{fl} contributes 10-20% of the entire brush height ($20 \leq N \leq 100$; $N \mathrel{\widehat{=}}$ degree of polymerization).[18]

The "grafting from" approach also leads to high grafting densities of $\sigma \rightarrow 1$ nm^{-2} which is the approximate limit for σ corresponding to the maximum achievable surface coverage of randomly arranged spheres at a planar surface.[19]

At medium and low grafting densities binary interactions between neighboring chains dominate the interaction free energy. In the high coverage regime additional three-body interac-

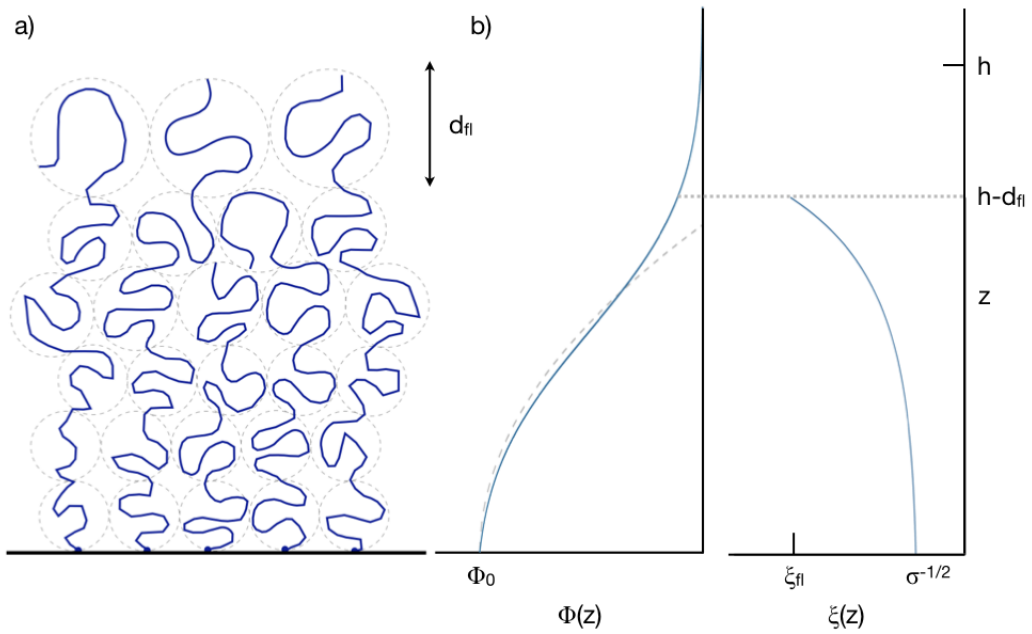

Figure 1: a) Scheme of a polymer brush. The dashed circles represent blobs, which increase in size as the distance from the grafting interface increases. This is shown in b), where the polymer volume fraction $\Phi(z)$ and the correlation length (blob size) ξ are schematically displayed against the distance from the grafting interface z. d_{fl} and ξ_{fl} are the diameter and the correlation length of the last blob respectively. Φ_0 is the polymer volume fraction at $z = 0$.[18]

tions have to be considered.[20–22]

In this regime the polymer volume fraction profile $\Phi(z)$ is predicted to be elliptic rather than parabolic

$$\Phi(z) = \Phi(0)[1 - (z/h)^2]^{1/2} \tag{4}$$

with $h = (2/\sqrt{\pi})Na^2/d$. Here N is the degree of polymerization ($M_n = N \cdot M_{mon}$), a the size of a monomer unit and M_{mon} the molar mass of a monomer unit.[21,23]

Also for long chain brushes at high grafting densities the parabolic regime changes to a more quasirectangular profile.[22]

Due to experimental conditions and high grafting densities, we assume that no expulsion of polymer chains due to degrafting events occurs during our GINSES measurements.[24,25] Therefore, we observe small deformations of the equilibrium structure of a transitionally invariant brush attached to an impenetrable planar solid substrate and the z-axis is the coordinate under observation. This means that transverse shear modes will not be addressed by the presented experiments, but rather longitudinal breathing modes that can be described by a cooperative diffusion coefficient D_{coop}

$$D_{coop} = \frac{k_B T}{(6\pi\eta_0 d)} \tag{5}$$

with η_0 the solvent viscosity and d the characteristic size ($\sim$ blob size ξ) in the brush.[26] While $d = const$ for an Alexander-de Gennes type brush, for a real brush we find that $d = f(z)$. It is expected that the local brush dynamics obey the balancing of the elastic restoring force and the viscous friction due to the solvent flow according to

$$\frac{\delta}{\delta z}\left[E(z)\frac{\delta u}{\delta z}\right] \approx \frac{\eta}{\xi^2(z)}\frac{\delta u}{\delta t} \tag{6}$$

with $u(z)$ the component of the displacement field under observation, η is the solvent viscosity and $\delta u/\delta z$ the strain, which for small longitudinal deformations is proportional to

the stress *P(z)*.[17] In an Alexander type brush the local correlation length is similar to the square root of the grafting density ($\xi(z) \approx 1/\sigma^{1/2}$). Therefore, the breathing modes can be described by a diffusion type equation

$$\frac{k_B T}{\eta \sigma^{1/2}} \frac{\delta^2 u}{\delta z^2} = \frac{\delta u}{\delta t} \tag{7}$$

where $k_B T/\eta\sigma^{1/2}$ is the diffusion constant of a single blob. This leads to a characteristic time τ_h for the longitudinal breathing modes according to

$$\tau_h \sim h^{-2} \sim N^2(\sigma/a^2)^{1/3} \tag{8}$$

With increasing distance from the grafting surface the relaxation time increases as well. However, this does not indicate that monomers towards the edge of the brush are slower, but that the magnitude of the fluctuations increases. While the motion of the polymer chains near the solid wall is constrained, the free end-displacements behave like free polymer segments in the dilute regime.

In the high grafting density regime stretching of the chains might lead to a decrease of the blob size.[27,28] Theoretical studies predict an increase of the relaxation times of fluctuations perpendicular to the grafting surface at increasing grafting densities.
The outer ends of the grafted chains dive down into the central brush interior. These calculations show that this process becomes increasingly inhibited when the grafting density reaches the high grafting density regime. This hindrance may result from an energetic barrier due to the increasing rigidity of the brush in this regime.[27]

In this paper PNIPAM brushes with different grafting densities were investigated. In the first part of the paper, structural features are probed using ellipsometry and neutron reflectometry. The influence of the grafting density on the swelling behavior of the PNIPAM brushes is presented. The grafting density is experimentally determined with size exclusion

chromatography (SEC), which also yields information about the molecular dispersity $Đ$ of the PNIPAM brushes. In the second part of the paper, the brush dynamics are observed with neutron spin echo spectroscopy under grazing incidence conditions. This allows the investigation of different layers of the PNIPAM brush by variation of the neutron penetration depth $z_{1/e}$. Here we were able to investigate Fourier times τ_{NSE} up to 60 ns. Furthermore, to reduce unavoidable inherent ambiguities in the determination of the experimental background in grazing incidence experiments, simulations of the transmitted and reflected intensities under total external reflection on the Distorted Wave Born Approximation (DWBA) implemented in the BornAgain software package are used in the data treatment.

Experimental

Materials

Copper(I) chloride (99.995%, trace metal basis), *N*-isopropylacrylamide (NIPAM, $\geq$ 99%), *N*, *N*, *N'*, *N"*, *N"*-pentamethyldiethylenetriamine (PMDETA, $\geq$ 99%), trichlorododecylsilane ($\geq$ 95% (GC)) tetrabutylammonium fluoride solution (1 M in THF) and tetrahydrofuran (THF, anhydrous $\geq$ 99.9% inhibitor-free) were purchased from Sigma-Aldrich. Hydrogen peroxide solution (30%), methanol (z.A. min. 99.8% CH_2OH) and sulfuric acid (z.A. 95%) were purchased from CHEMSOLUTE®. Toluene (dried, max. 0.005% H_2O) was purchased from SeccoSolv®. Ethanol (absolute) was purchased from VWR CHEMICALS. [11-(2-Bromo-2-methyl)propionyloxy]undecyltrichlorosilane (eBMPUS) was purchased from Gelest. Deuterium oxide (99.9%) was purchased from Deutero GmbH. Water was purified with a MilliQ system (Millipore) with a resistance of 18 MΩ·cm.

Synthesis of PNIPAM brushes

The synthesis of PNIPAM brushes is adapted from the literature.[29,30] However, some modifications were made as described below.

All silicon substrates were etched with Piranha solution (i.e., H_2SO_4:H_2O_2 1:1 v/v%) for 30 min, thoroughly rinsed with MilliQ water and dried under a stream of nitrogen.

To apply a self-assembled monolayer (SAM) of [11-(2-Bromo-2-methyl)propionyloxy]undecyl trichlorosilane (eBMPUS), 45 mL of anhydrous toluene was transferred into a glass reactor and purged with nitrogen for 30 min. A 5 wt% solution of eBMPUS in anhydrous toluene (45 μL) was then added under nitrogen bubbling and after 5 min the etched silicon substrates were placed in the reactor. The reactor was sealed air tight and protected from light with aluminium foil. The reaction was carried out for 24 h at room temperature. Afterwards, the substrates were sonicated in toluene for 15 min and in ethanol for 5 min and dried under a stream of nitrogen to remove excess reactant. The grafting density was varied by the addition of trichlorododecylsilane to the eBMPUS solution during SAM deposition. While the molecular structure of this "dummy" molecule resembles that of the initiator (Figure S1), it is not able to initiate polymerization.[31,32]

PNIPAM brushes were grafted from silicon substrates via surface-initiated atom transfer radical polymerization (SI ATRP). NIPAM (2.0 g, 17.67 mmol (1.0 g, 8.84 mmol for slower kinetics)) was dissolved in 23 mL methanol and 23 mL MilliQ water under nitrogen bubbling and continuous stirring (500 rpm). After 30 min the ligand PMDETA (150 μL, 0.718 μmol) and activating species Cu(I)Cl (0.0195 g, 0.197 mmol) were added and the solution was purged with nitrogen and stirred for another 30 min. Afterwards, the stirring bar was removed and the substrates with the SAM were placed in the SI ATRP solution. For kinetic samples, substrates were removed after different polymerization times.

For removal of excess reactant the substrates were sonicated in MilliQ water for 5 min and dried under a stream of nitrogen.

For laboratory scale experiments PNIPAM brushes were grafted from silicon wafers (2 cm x 2 cm). For neutron scattering experiments the experimental conditions were upscaled sixfold and PNIPAM brushes were grafted from silicon blocks (5 cm x 8 cm x 1.5 cm).

Concerning the grafting density, experimental conditions during SAM deposition should lead to the same grafting densities on silicon wafers and silicon blocks, if the same molar ratio of initiator and dummy molecules is chosen.

Nomenclature of the used samples follows the scheme "PNIPAM-substrate-molar ratio dummy-polymerization time in seconds", where B = silicon block and W = silicon wafer. For example "PNIPAM-B-0.2-240" is a PNIPAM brush grafted from a silicon block with a molar ratio of dummy of 0.2 that was polymerized for 240 s.

Degrafting of PNIPAM brushes

To determine their average molar mass M_n, molecular dispersity $Đ$ and grafting density σ PNIPAM brushes were degrafted with tetrabutylammonium fluoride (TBAF) as displayed in Figure 2.[33] First, SI ATRP as described above was carried out on a total of 16 double side polished (DSP) Si wafers (2 cm x 2 cm per wafer) to maximize the yield and ensure enough material for SEC. The degrafting procedure was carried out in a cleanroom and all solvents were filtered through two polytetrafluoroethylene (PTFE) filters (2 μm and 0.2 μm). A filtered solution of TBAF in THF (0.04 M) was placed in a double-walled glass reactor and all 16 DSP Si wafers were added in a PTFE holder. The reactor was sealed airtight and the mantle was heated to 50 °C. The degrafting proceeded for 24 h. Afterwards, the Si wafers were removed from the reactor, thoroughly rinsed with filtered THF and measured with X-ray reflectometry (XRR) to ensure complete removal of the PNIPAM brushes. THF was then removed with a rotary evaporator and the brown resin was lyophilized. The resin was redissolved in filtered MilliQ water and dialyzed for a week with daily water exchange (MWCO = 6-8 kDa) to remove any excess TBAF. The dialysis was carried out at 4 °C to ensure the stretched state of the PNIPAM chains. After dialysis the solution was again lyophilized and a brown resin was received, which was then measured with SEC. Chromatograms can be found in the SI section.

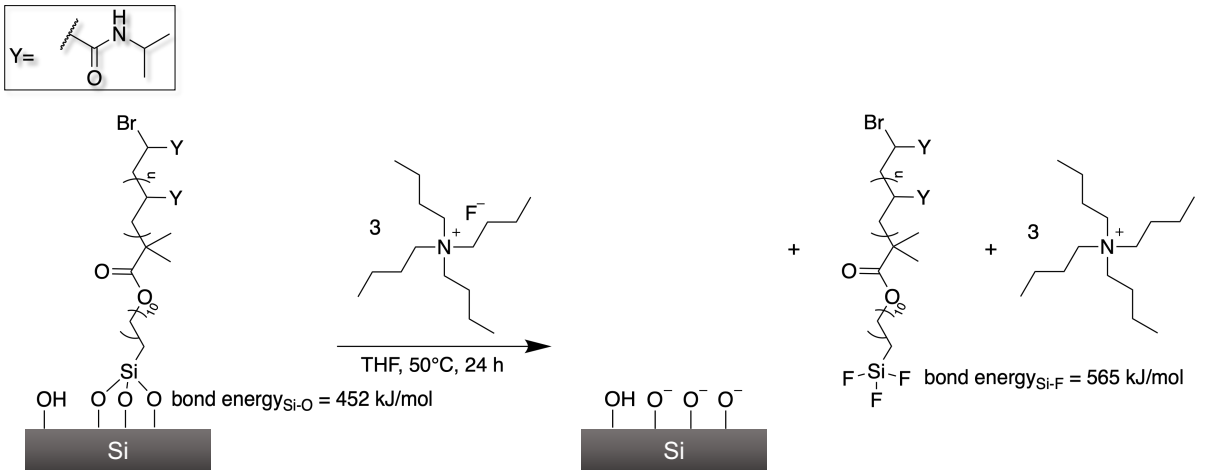

Figure 2: Reaction scheme of the degrafting of PNIPAM brushes from SiO_2 substrates using TBAF. The reaction is driven by the higher bond energy of a Si-F bond (565 kJ/mol) compared to Si-O (452 kJ/mol). A more detailed description can be found in the literature.[33]

Ellipsometry

Ellipsometry was used to determine the dry and swollen thickness of PNIPAM brush layers. Furthermore, the refractive index of the PNIPAM brush layers in the swollen state was determined. A Multiscope Null-Ellipsometer (Optrel GbR, Germany) equipped with a green laser ($\lambda = 532$ nm) and a PCSA (polarizer-compensator-sample-analyzer) setup was used. For dry measurements an angle of incidence α_i of 70° was chosen. The relative humidity during dry measurements was 30 to 40%. For measurements in water the sample was placed in a stainless steel cell filled with MilliQ water and mounted on top of the sample stage. Here α_i was 60°. The temperature of the sample cell was adjusted with a copper plate underneath the sample holder and a thermostat, in order to observe the temperature-dependent collapse of brushes with different heights and grafting densities. The obtained data was fitted with a 4-layer model with the following layers: (i) silicon substrate ($n = 4.1520, h = \infty$), (ii) fused silica ($n = 1.4607, h = 1.5\ nm$), (iiia) PNIPAM brush in air ($n = 1.5062, h = h_{\text{fit}}$), (iiib) PNIPAM brush in water ($n = n_{\text{fit}}, h = h_{\text{fit}}$) and (iva) air ($n = 1.00028381, d = \infty$) and (ivb) water ($n = 1.33370, d = \infty$).

Size Exclusion Chromatography

Size exclusion chromatography (SEC) measurements were carried out at the Max Planck Institute of Colloids and Interfaces in Golm, Germany. A series of three columns (PSS GRAM VS, PSS GRAM 7 μm, 100 Å and PSS GRAM 7 μm, 1000 Å) calibrated with PS standards was used. *N*-methylpyrrolidone (NMP) with 0.5 g/L LiBr was the eluent at a temperature of 70 °C and a flow rate of 0.8 mL/min. A PSS SECcurity UV and RI (RI $\widehat{=}$ refractive index) detector were used. The setup was calibrated for a molar mass range of 600 - 2 000 000 g/mol.

Neutron Reflectometry

Neutron reflectometry (NR) measurements were conducted at the Magnetic Reflectometer with High Incidence Angle (MARIA, MLZ, Garching, Germany).[34] Measurements were carried out in non-polarized beam mode at a wavelength of $\lambda = 10$ Å for low Q-values and $\lambda = 5$ Å for higher Q-values, with a wavelength distribution of $\Delta\lambda/\lambda = 0.1$. Samples were measured in a custom made sample cell, consisting of two aluminium blocks for temperature control which enclose a PTFE trough and the silicon block. The PTFE trough was filled with D_2O and measurements were conducted at 15 °C and 50 °C. Neutron reflectivity curves for measurements at 50 °C are displayed in Figure S6.

Neutron reflectometry data for PNIPAM-B-0-120 was fitted with a three-layer model. Here, the first layer is the silicon oxide layer with an SLD of $3.47 \cdot 10^{-6}$ Å^{-2} and a thickness of 1.5 nm, while the second layer is composed of the initiator SAM with a SLD of $0.29 \cdot 10^{-6}$ Å^{-2} and a thickness of 1.3 nm. The third layer is the PNIPAM brush. The SLD for PNIPAM was taken from the literature as $0.8 \cdot 10^{-6}$ Å^{-2}. The initial guess for the thickness of the brush layer is estimated from ellipsometry measurements.

For PNIPAM-B-0.2-240 at 15 °C we assumed a four-layer model, referring to earlier results by Brouette et al.[35] We justify this by the comparable brush samples. In contrast to

the above mentioned three-layer model an additional brush layer towards the D_2O layer with a higher solvent content is added. In this context the solvent content describes the volume fraction of D_2O (solvent) in the respective layer (e.g. brush). Furthermore, the SLD of the initiator SAM is adjusted to the ratio of initiator to dummy molecules.

Grazing Incidence Neutron Spin Echo Spectroscopy

Grazing incidence neutron spin echo spectroscopy (GINSES) experiments were carried out on the J-NSE instrument (MLZ, Garching, Germany).[36] An illustration of the GINSES scattering geometry is displayed in Figure 3. Detailed descriptions of the sample cell and experimental setup are found elsewhere.[12,13] It is important to mention that the in-plane component of the scattering vector $Q_{GINSES} = k_{det} - k_i$ is negligible compared to the much larger z-component. This is because for polymer brushes with their chain length distribution and lateral homogeneous polymer density no significant lateral correlations in the range of a few ten nanometers are expected.[12] Neutron wavelengths of $\lambda = 6$ Å and $\lambda = 8$ Å ($\Delta\lambda/\lambda = 0.2$) were used and all measurements were conducted at 15 °C. The scattering geometry is shown in Figure 3. The angle of incidence α_i was varied to measure at different neutron penetration depths $z_{1/e}$. The neutron penetration depth describes the characteristic distance perpendicular to the surface at which the intensity of the evanescent wave drops to 1/e.[37] Most importantly, the critical angle of total reflection α_c depends on the neutron wavelength λ and the scattering length density contrast $\Delta\rho$ according to

$$\alpha_c = \lambda\sqrt{\Delta\rho/\pi} \tag{9}$$

The value of α_c was taken from the position of the critical edge of total reflection in the neutron reflectivity curves and recalculated for the neutron wavelength of the GINSES experiment.

In the grazing incidence geometry the generation of an evanescent neutron wave at an angle

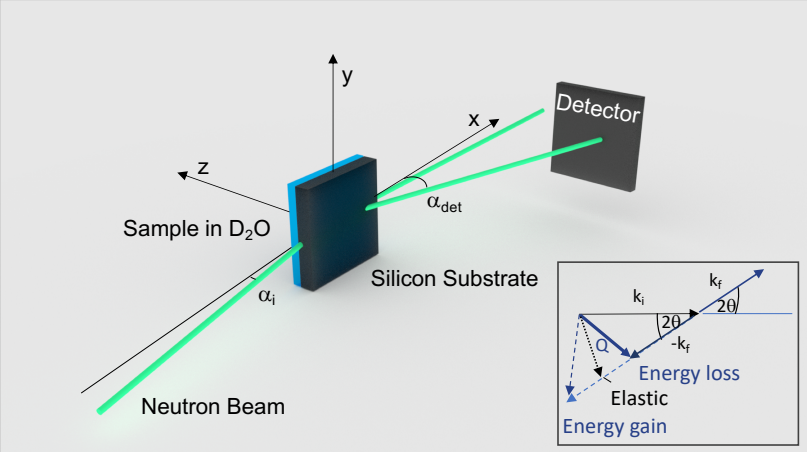

Figure 3: Schematic setup of a GINSES experiment. The inset shows the scattering wavevector for inelastic scattering. The neutron beam enters from the silicon substrate and is reflected at the brush-silicon oxide interface.

of incidence α_i below the critical angle of total reflection α_c ($\alpha_i < \alpha_c$) with a certain intensity $I_{ev}(z) = I_{ev,max} exp(-z_{1/e}/z)$[37] is used to penetrate into the sample layer at a chosen penetration depth $z_{1/e}$, which can be calculated according to

$$z_{1/e} = \frac{2^{\frac{1}{2}}\lambda}{4\pi\{[(\alpha_i^2 - \alpha_c^2)^2 + (\frac{\lambda\mu}{2\pi})^2]^{\frac{1}{2}} - (\alpha_i^2 - \alpha_c^2)\}^{\frac{1}{2}}} \tag{10}$$

Absorption is taken into account by μ, the absorption coefficient, given by the total scattering cross section σ_{tot} per volume σ_{tot}/V.[37] Details about the calculation can be found in Table S1.

Figure 4 shows the neutron penetration depths for both investigated brush samples measured in the grazing incidence scattering geometry depicted in Figure 3. The parameters of the calculation of $z_{1/e}$ according to eq 10 are summarized in Table 1.

Since grazing incidence measurements suffer from low signal intensity, the reasonable Q-range for the measurements was identified by a Q-scan of the scattered intensity in reflection mode. This is shown in Figure S9 in the supporting information. Considering the coherently scattered intensity in the spin-up configuration of the instrument and the incoherently

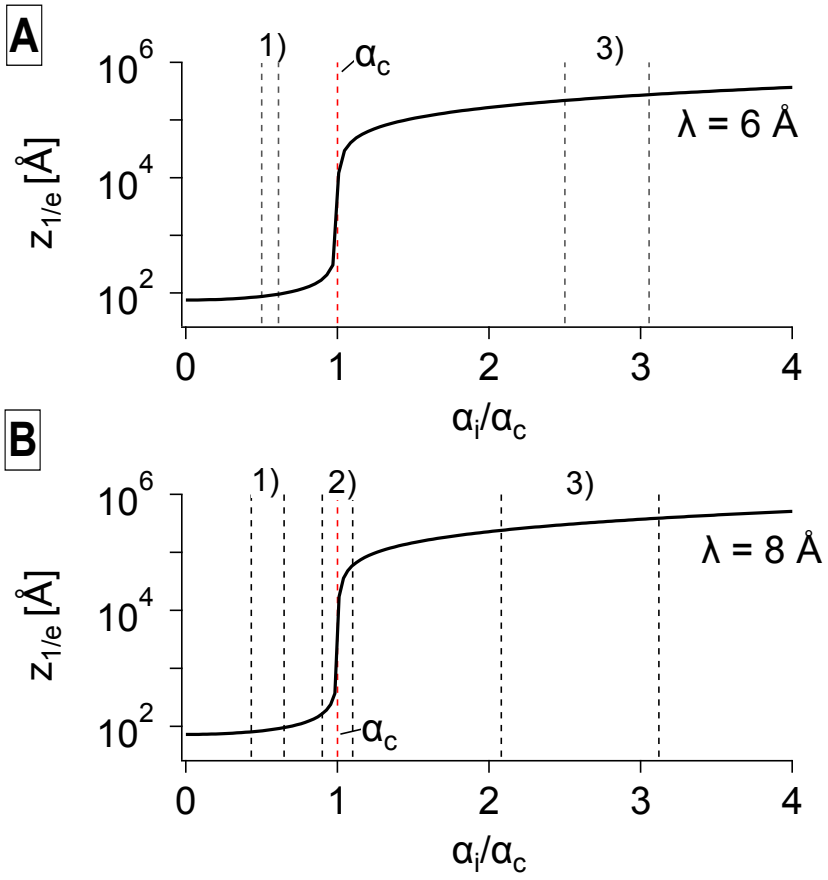

Figure 4: Neutron penetration depths for PNIPAM-B-0-120 (A) and PNIPAM-B-0.2-240 (B) calculated according to eq 10. The angle of incidence α_i was normalized with the critical angle α_c. The red dashed lines mark the critical angle α_c determined from neutron reflectometry measurements. The black dashed lines show the range in which measurements were taken due to the wavelength distribution of 20%. 1) Evanescent regime ($\alpha_i < \alpha_c$), typically 10 - 100 nm, 2) $\alpha_i \approx \alpha_c$ transition from evanescent regime to transmission regime, typically a wide range of $z_{1/e}$, 3) transmission regime $\alpha_i \gg \alpha_c$ with virtually infinite penetration depth.

Table 1: Neutron penetration depths $z_{1/e}$ calculated according to eq 10. $z_{1/e,min}$ is the minimum neutron penetration depth and $z_{1/e,max}$ the maximum neutron penetration depth taking into consideration a wavelength distribution $\Delta\lambda/\lambda$=0.2.

Sample	α_i	α_c	$z_{1/e,min}$ (nm)	$z_{1/e,max}$ (nm)
PNIPAM-B-0-120	0.2°	0.44°	8.78	9.7
PNIPAM-B-0-120	1.0°	0.44°	22000	28000
PNIPAM-B-0.2-240	0.27°	0.58°	8.0	9.5
PNIPAM-B-0.2-240	0.5°	0.58°	16.5	5817
PNIPAM-B-0.2-240	1.3°	0.58°	24000	39000

scattered neutrons (background) measured in the spin-down configuration, the accessible Q-range is limited to low Q-values. Hence, $Q_{GINSES} = 0.06$ Å^{-1} was chosen for the GINSES measurements.

Since the dynamics of a sample under study is measured as a function of time, NSE and GINSES yield the intermediate scattering functions S(Q, τ_{NSE}). The time parameter τ_{NSE} is an instrumental parameter with the dimension of time called "Fourier time", being $\tau_{NSE} \propto \lambda^3 \cdot B$, where B is the absolute value of the magnetic field.[38]

The standard normalization procedure and background correction of NSE measurements in transmission mode cannot be applied for measurements in reflection mode. As can be seen from eq 9 the critical angle α_c intimately depends on the composition of the sample interface which changes when the brush sample is replaced by a bare silicon block. To circumvent this inherent difficulty and to estimate the background of the sample cell with and without the brush sample, BornAgain calculations were done as is explained below and in the SI section.

Modeling of the evanescent wave

To estimate the contributions of brush regions at different distances from the grafting surface to the measured scattering signal and the penetration depth $z_{1/e}$ of the evanescent neutrons, simulations using the BornAgain platform were performed within the framework of the Distorted Wave Born Approximation.[39] Simulations were used to numerically study the distribution of the evanescent intensity $I_{ev}(z, \alpha_i)$ at constant neutron wavelength and to compare the relative contributions of the solid-liquid interface with and without a brush sample layer to the experimentally observed elastic background in the scattering signal. The instrument resolution, layer roughness and absorption effects of each layer were included. As in the real physical experiment, in the simulations the neutron beam impinges on the interface through the silicon block. In the simulations, thickness parameter and SLD values were chosen according to the analysis of the neutron reflectivity measurements. The gradually changing scattering length density profiles of the brushes obtained in the Motofit analysis

of the neutron reflectivity measurements were sliced into 100 layers of different scattering length density values. The transition between the individual layers was adapted according to the polymer volume fraction profile given in eq 1. These approximations were slightly refined during the simulation runs to avoid mathematical instabilities and artificial contributions in the calculated intensity distribution. Further details are given in the SI section.

Results and discussion

Structure of PNIPAM brushes with different grafting densities

Characterization of brush height and swelling behavior with ellipsometry

As typically observed in SI ATRP the development of the brush height displays a linear dependence on the polymerization time t_p in the beginning stages of the polymerization, up to a leveling off as the polymer brush reaches its maximum height due to termination.[40,41] The dry brush height of the PNIPAM brushes synthesized for this paper for two different monomer concentrations (1 vs. 2 g) in dependence of t_p is displayed in Figure S2. Here, polymerization times between 1 and 4 minutes are displayed. It shows how a reduction of the monomer amount by half leads to slower brush growth reflected by a decrease in the slope and therefore better control over the polymerization. This is in agreement with theoretical expectations according to

$$R_p = k_p[M][P_n^{\cdot}] \tag{11}$$

where R_p is the rate of polymerization, k_p is the rate constant of the polymerization, $[M]$ the monomer concentration and $[P_n]$ the concentration of polymer radicals.[41]

While with 2 g NIPAM a polymer brush of 38 nm results after the first minute, the corresponding brush with 1 g NIPAM displays a height of 25 nm. After 4 min the difference is even more pronounced with 108 vs. 48 nm for 2 and 1 g NIPAM respectively.

The brush collapse of a shorter (PNIPAM-W-0-60, $t_p = 1$ min) and a longer (PNIPAM-W-0-180, $t_p = 3$ min) PNIPAM brush was monitored with ellipsometry. The degree of collapse α_{col} was calculated according to

$$\alpha_{col} = \frac{h(T) - h_{sw}(T_{ref})}{h_{sw}(T_{ref})} \tag{12}$$

where $h_{sw}(T_{ref})$ is the brush height in water at the reference temperature $T_{ref} = 15$ °C and $h(T)$ the brush height in water at a given temperature 15 °C $\leq T \leq$ 50 °C.[42] The resulting values are displayed in Figure 5.

In the context of this paper we refer to the brush in water at 15 °C as the "swollen" state, whereas the brush in water at 50 °C is referred to as being in the "collapsed" state. The brush in air, where no solvent is present, is referred to as the "dry" state.

The corresponding temperature-dependent ellipsometry measurements of the swollen brush in water are found in Figure S3.

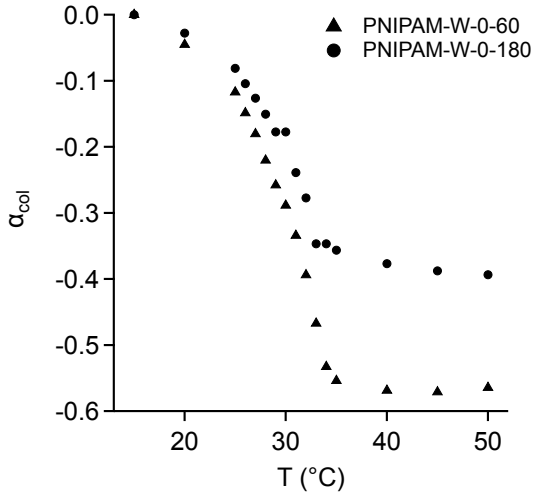

Figure 5: Degree of collapse α_{col} for PNIPAM brushes with two different polymerization times t_p; PNIPAM-W-0-60 (1 min), PNIPAM-W-0-180 (3 min). Calculated according to eq 12 from ellipsometry measurements in water.

Figure 5 shows a more pronounced collapse for the initially thinner PNIPAM-W-0-60 with $\alpha_{col} = -0.57$ compared to the thicker PNIPAM-W-0-180 with $\alpha_{col} = -0.39$. This

is in agreement with findings by Yim et al.,[32] who found that at high grafting densities the ratio of the first moment of the segment concentration profile at 20 and 40 °C decreased with increasing molar mass of the polymer chains.

The results of our ellipsometry measurements are displayed in Table 2. The dry brush height for the maximum grafting density at different polymerization times (PNIPAM-W-0-60 and PNIPAM-W-0-180) is 38 nm after 60 s and 91 nm after 180 s. In water the thickness at 15 °C increases to 90 nm for PNIPAM-W-0-60 and to 153 nm for PNIPAM-W-0-180. Upon increasing the temperature to 50 °C the brush collapses to 39 nm and 93 nm respectively. This collapse is expressed with the above mentioned degree of collapse.

Furthermore, ellipsometry was measured on a PNIPAM brush with a varied grafting density, where the molar ratio of initiator and dummy molecules was 1 to 0.2. This brush might be described as a semidilute brush. It shows thermoresponsive behavior similar to the maximum grafting density brush with a molar ratio of 1 to 0 between initiator and dummy molecules. In the swollen state PNIPAM-W-0.2-240 has a swollen height of 68 nm and a degree of collapse of $\alpha_{col} = -0.48$. Moreover, the change of refractive index towards the value of the pure polymer gives another qualitative indicator for the expelling of water from the PNIPAM brush layer ($n_{H_2O} = 1.33, n_{PNIPAM} = 1.52$).

Our results qualitatively agree with previous studies on PNIPAM brushes using spectroscopic ellipsometry. While we applied classical Null ellipsometry at a single optical wavelength to characterize the brush height, we had to keep the fitting models simple to avoid incorrect interpretation of the data due to ambiguities in the fitting process. Hence, our results give reliable values of the heights in the dry and collapsed wet state, but estimate the brush height in the swollen state. However, our results agree with measurements by Kooij et al.[43] and Yu et al.[44] who used spectroscopic ellipsometry for the brush characterization. Hence, Kooij et al. were able to measure rather detailed refractive index profiles of PNIPAM brushes in water at different grafting densities.

Table 2: Thickness h and refractive index n of PNIPAM brushes with different grafting densities as measured with ellipsometry. Refractive index in the dry state taken from Reufer et al.[45] The collapse ratio α_{col} was calculated according to eq 12.

Sample	T (°C)	h (nm)	$n_{532.6\ \mathrm{nm}}$	α_{col}
PNIPAM-W-0-60$_{dry}$	r.t.	38 ± 0.6	1.52 ± 0.01	
PNIPAM-W-0-60$_{wet}$	15	90 ± 0.02	1.3844	
PNIPAM-W-0-60$_{wet}$	50	39 ± 0.03	1.4552	-0.57
PNIPAM-W-0-180$_{dry}$	r.t.	91 ± 1.1	1.52 ± 0.01	
PNIPAM-W-0-180$_{wet}$	15	153 ± 0.01	1.3794	
PNIPAM-W-0-180$_{wet}$	50	93 ± 0.02	1.4732	-0.39
PNIPAM-W-0.2-240$_{dry}$	r.t.	29 ± 0.3	1.52 ± 0.01	
PNIPAM-W-0.2-240$_{wet}$	15	68 ± 0.08	1.3925	
PNIPAM-W-0.2-240$_{wet}$	50	33 ± 0.25	1.4548	-0.52

Degrafting for the determination of M_n, $Đ$ and σ

In order to ensure the synthesis of PNIPAM brushes with different grafting densities yields polymer chains with similar molar mass and molar mass distribution, SI ATRP grafted PNIPAM brushes were cleaved from Si substrates as described in the methods section. Size exclusion chromatograms as presented in Figures S4 and S5 show that the maximum grafting density yields polymer chains with $M_n = 40500$ g/mol after a total polymerization time $t_p = 120$ s, which is comparable to $M_n = 46500$ g/mol for the minimum grafting density after $t_p = 240$ s. Furthermore, both samples display a molecular dispersity of $Đ = 1.5$. It should be mentioned that we base our analysis on the signal from the UV detector, since the RI detector signal is concentration dependent and degrafting yields rather low sample amounts.

We find a bimodal molar mass distribution for both samples with one peak at low molecular masses ($M_n = 1300$ g/mol for maximum and $M_n = 2700$ g/mol for minimum grafting density) and another one at higher molar masses expected for a polymer chain in a brush layer of the measured dry thickness. This has been observed in the past by Pasetto et al.[46] in PS and PMMA brushes and is attributed to termination by disproportionation, where Pasetto et al. found saturated and unsaturated chain ends, the products of such disproportionation. Because of the bimodal molar mass distribution, the values for the grafting densities calcu-

lated from

$$\sigma = \frac{\rho_M N_A h_{dry}}{M_n} \tag{13}$$

with σ the grafting density, ρ_M the density of the monomer, N_A Avogadro's number, h_{dry} the dry thickness of the polymer brush and M_n the molecular mass of the polymer chain, can only be regarded as approximations to the actual grafting densities. This yields grafting densities of $\sigma = 0.6$ nm^{-2} and $\sigma = 1.0$ nm^{-2}. Considering the experimental uncertainty and in comparison to values reported in the literature, we attribute our brushes to the semidilute and concentrated regime.

To characterize the tethering regime of grafted polymers the so called reduced tethered density $\Sigma = \sigma\pi R_g^2$ is used. This yields the number of grafted chains in the cross-sectional area of the free polymer chains in bulk. Values of $\Sigma < 1$ correspond to the mushroom regime, at $\Sigma \approx 1$ the transition into the brush regime occurs which is fully established at $\Sigma >> 1$.[47] The large values of Σ clearly indicate that these brushes are in the highly stretched regime in the range of very large grafting densities ($\sigma \to 1$) and medium chain lengths ($N \approx$ 160-400) studied here.

From the grafting densities determined from DSP Si wafers and dry thicknesses measured with ellipsometry on the block samples PNIPAM-B-0-120 and PNIPAM-B-0.2-240 we were able to calculate the molar mass M_n, degree of polymerization N and reduced grafting density Σ for those block samples (Table 3).

Table 3: Grafting density σ, dry brush height h_{dry} measured with ellipsometry, molar mass M_n calculated according to eq 13, degree of polymerization N and reduced grafting density Σ for PNIPAM brushes grafted from Si blocks. These samples were used for all neutron studies in this publication.

Sample	σ (nm^{-2})	h_{dry} (nm)	M_n (g/mol)	N	Σ
PNIPAM-B-0-120	1.0	42	28000	250	190
PNIPAM-B-0.2-240	0.6	27	18000	160	70

While the resulting values for Σ are smaller than on the DSP Si wafers they still show that our samples are in the fully established brush regime where $\Sigma >> 1$.

Neutron reflectometry measurements

Figure 6 displays neutron reflectivity curves of PNIPAM-B-0-120 and PNIPAM-B-0.2-240 in the swollen state at 15 $°C$. The curves were fitted with layer models as described in the materials section. Neutron reflectivity curves in the collapsed state at 50 $°C$ were measured as well and are displayed in the SI section.

In the swollen state (i.e. at 15 $°C$) the resulting reflectivity curves do not display distinct Kiessig fringes (Figure 6), since there is a rather smooth transition between the PNIPAM brush and the solvent (D_2O). As described above for PNIPAM-B-0-120, the sample with a maximum grafting density, the reflectivity curve could be fitted with a single PNIPAM brush layer. The resulting layer has a thickness of 81 nm and a solvent content of 51% v/v. From the fit of the same sample at 50 $°C$ the collapse becomes apparent in the decrease of layer thickness to 54 nm and repulsion of solvent to a solvent content of 38% v/v (Table 4).
In the case of a lower grafting density (PNIPAM-B-0.2-240) the PNIPAM layer could be subdivided into two layers with different solvent content. A single layer model did not lead to physically plausible results. The layer closer to the substrate is thinner and displays a lower solvent content of 38% v/v than the layer in closer proximity to the bulk phase with 86% v/v. These results are mirrored in the SLD profiles calculated from the fits (see Figure S6). From the SLD profiles the polymer volume fractions were calculated assuming additivity of the contributions from polymer and D_2O.

The polymer volume fraction (PVF) profiles at 15 $°C$ illustrate the smooth transition from the PNIPAM brush into the solvent. A detailed list of all fit parameters is found in Table 4.

For the lower grafting density (PNIPAM-B-0.2-240) in the swollen state, i.e. at 15 °C, there

is a dense inner layer and a more dilute outer layer with a chain end segment distribution. At 50 °C this outer layer collapses onto the dense inner layer, which apparently increases in thickness (20 to 28 nm) and the water content of this layer decreases slightly. However, in the region of layer 2 there is a pronounced increase in the PVF, accompanied by a strong decrease of the water content (86 %v/v to 35 %v/v). In very close proximity to the substrate the PVF does not change significantly (within the precision of the neutron reflectometry measurement). We assume that this is due to steric reasons due to the collapse of layer 2.

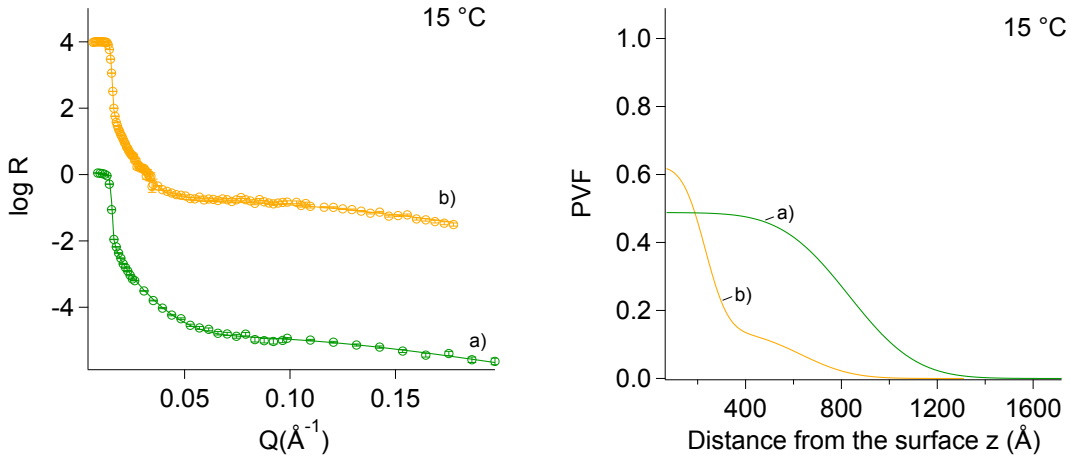

Figure 6: Left: Neutron reflectivity curves and corresponding fits of a)PNIPAM-B-0-120 and b)PNIPAM-B-0.2-240 at 15 °C in D_2O. Right: Corresponding polymer volume fraction (PVF) profiles calculated from SLD profiles (Figure S6).

Previous reports of neutron reflectometry measurements on PNIPAM brushes are in good agreement with these findings.[32,35] Similar observations were also made in force measurements between PNIPAM brushes and mica surfaces in a wide range of molar masses and grafting densities. A dense PNIPAM layer in the vicinity of a hydrophilic surface due to attractive polymer-surface interactions was subsequently followed by a less dense layer passing over into the aqueous bulk phase. Our findings furthermore are in agreement with theoretical studies by Descas et al.[48] and experimental results from Kooij et al.[43] and Yu et al.[44] who, using spectroscopic ellipsometry, found an optically dense film in PNIPAM brushes at the substrate film interface and a more diluted layer on top.[43]

Table 4: Thickness h, D_2O penetration and roughness of PNIPAM brushes with different grafting densities (σ = 0.6 *and* 1.0 nm^{-2}) as determined with neutron reflectometry. Here α_{col} was determined from h values measured with NR.

Sample	T (°C)	h (nm)		D_2O (%v/v)		roughness (nm)		α_{col}
		Layer 1	Layer 2	Layer 1	Layer 2	Layer 1	Layer 2	
PNIPAM-B-0-120$_{dry}$	r.t.	42	-	-	-	-	-	
PNIPAM-B-0-120$_{wet}$	15	81	-	51	-	22	-	
PNIPAM-B-0-120$_{wet}$	50	54	-	38	-	1.6	-	-0.33
PNIPAM-B-0.2-240$_{dry}$	r.t.	27	-	-	-	-	-	
PNIPAM-B-0.2-240$_{wet}$	15	20	40	38	86	7.4	17	
PNIPAM-B-0.2-240$_{wet}$	50	28	-	35	-	1.3	-	-0.53

Dynamics of PNIPAM brushes of different grafting densities

Calculation of the evanescent intensity distribution

In contrast to NSE in transmission mode, under grazing incidence conditions, no standard background correction is possible, since the critical angle and therefore the neutron penetration depth strongly depend on the scattering length density contrast at the solid-liquid interface. To minimize the uncertainty of the background determination during the fitting process, numerical simulations using the BornAgain software were performed. Figure 7 shows the two-dimensional distribution of the evanescent intensity for PNIPAM-B-0-120 immersed in D_2O in the swollen state being based on the PVF distributions obtained from the neutron reflectometry measurements. In Figure 7 the variation of the evanescent intensity distribution is mapped in dependence of the angle of incidence α_i of the impinging neutrons and the distance from the scattering plane (Zero marks the scattering plane, values below refer to positions inside the silicon subphase and distance is the vertical position perpendicular to the substrate.) In the evanescent regime below the critical angle of total external reflection α_c, at increasing values of the angle of incidence α_i the evanescent neutrons extend further into the sample. Above α_c the neutron penetration depth extends to virtual infinity. Cuts through this intensity map at constant α_i allow to estimate the neutron penetration depth

$z_{1/e}$ under these particular scattering conditions. This is shown on the right in Figure 7 for sample PNIPAM-B-0-120. According to these cuts, for $z_{1/e}$ values of 25 nm and 16 nm were yielded for samples PNIPAM-B-0-120 and PNIPAM-B-0.2-240 respectively. These values are by a factor of 2-3 larger than the estimations according to eq 10. However, these values agree with the finding that under the chosen scattering conditions an interfacial region up to twenty to thirty percent of the brush height was probed.

Moreover, simulations of the scattering intensity under grazing incidence conditions for the brush-silicon interface and the D_2O-silicon interface yield an estimation of the contribution of the substrate (Figure S8) to the elastic background in the scattering signal (Figure S7). The elastic background is a superposition of an elastic signal from the polymer brush itself and the background stemming from the silicon substrate.

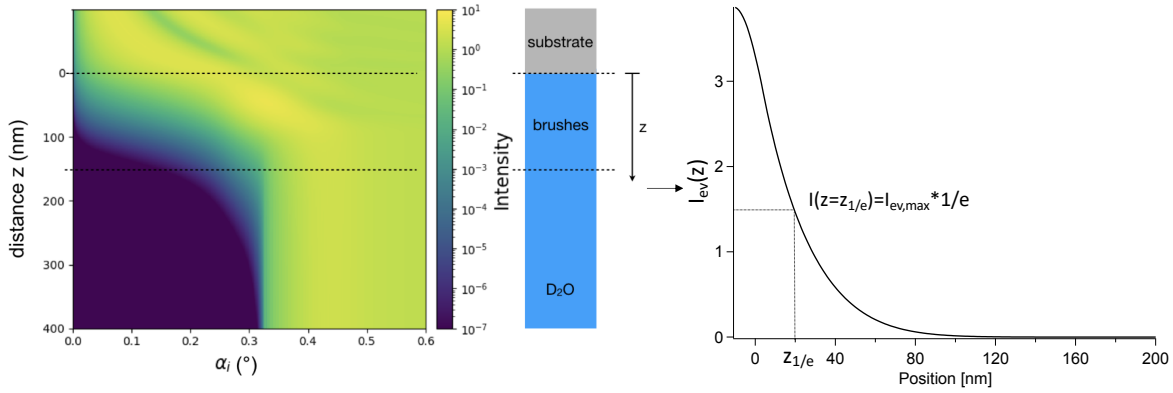

Figure 7: Left: Two-dimensional distribution of the evanescent intensity for PNIPAM-B-0-120 immersed in D_2O in the swollen state at 15 $°C$. Mapped is the variation of the evanescent intensity as a function of the angle of incidence α_i of the impinging neutrons and the distance from the scattering plane (Zero marks the scattering plane, values below refer to positions inside the silicon subphase and distance is the vertical position perpendicular to the substrate.) Right: Vertical line cut of the intensity map of PNIPAM-B-0-120 at $\alpha_i = 0.2°$.

Grazing incidence NSE measurements

Neutron spin echo spectroscopy experiments under grazing incidence geometry (GINSES) were performed under different angles of incidence α_i to probe different neutron penetration depths into the sample parallel to the interface between substrate and PNIPAM brush. The

neutron penetration depth $z_{1/e}$ was calculated according to eq 10 for different angles of incidence and is displayed in Figure 4.

Q-scans for each sample were conducted to determine a Q_{GINSES}-value suitable for the GINSES measurements. These Q_{GINSES}-scans are displayed in Figure S9. Finally, a Q_{GINSES}-value of 0.06 Å^{-1} was chosen for all samples and all angles of incidence. For data analysis the background A_{bgr} , which sums up elastic scattering and the experimental background was determined from measurements of the sample cell with an uncoated silicon block against D_2O (see Figures S7 and S8) and the numerical calculations. Therefore, GINSES data was first fitted according to

$$S(Q, \tau_{NSE}) = (A - A_{bgr})e^{-\Gamma_c \tau_{NSE}} + A_{bgr} \tag{14}$$

with $(A - A_{bgr})$ the amplitude, consisting of the density fluctuations of the polymer segments and the background A_{bgr} as described above. Γ_c is the relaxation rate attributed to the coherent signal and τ_{NSE} the Fourier time parameter from the GINSES measurements. Furthermore, we observed an initial incline of the intermediate scattering function at lower Fourier times for low penetration depths in the semidilute brush sample. This initial incline we ascribe to incoherent scattering from hydrogen atoms in the sample. In those cases we extended eq 15 with a factor containing the incoherent relaxation rate Γ_i.

$$S(Q, \tau_{NSE}) = (A - A_{bgr})(1 - e^{-\Gamma_i \tau_{NSE}})e^{-\Gamma_c \tau_{NSE}} + A_{bgr} \tag{15}$$

From the fitted values for the coherent relaxation rates Γ_c the dynamic correlation length of the breathing modes of the PNIPAM brushes was calculated according to

$$\xi_{coop} = \frac{k_B T}{6\pi\eta_0(\Gamma_c/Q^2_{GINSES})} \tag{16}$$

where k_B is the Boltzman constant, T the temperature in K, η_0 the solvent viscosity and Q_{GINSES} the absolute value of the momentum transfer.

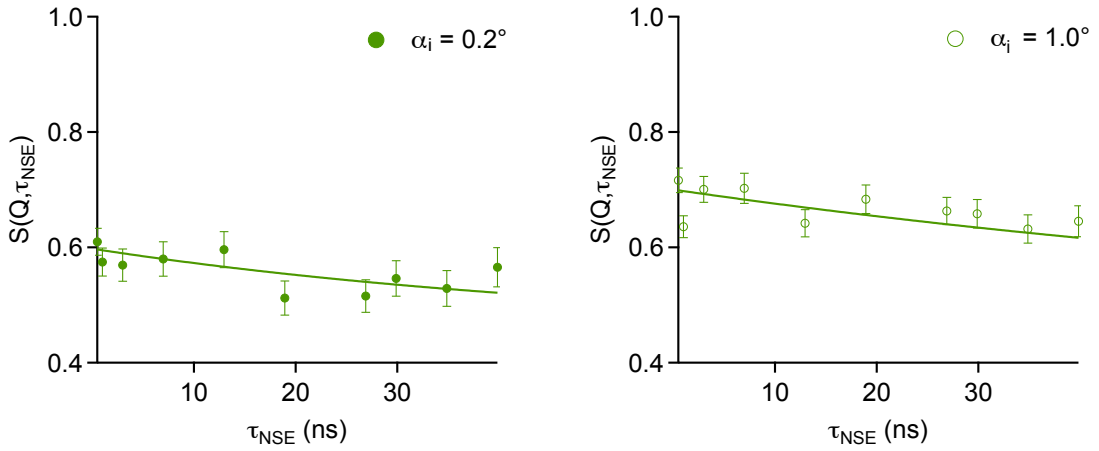

Figure 8: Intermediate scattering functions S(Q,τ_{NSE}) for PNIPAM-B-0-120 with a maximum grafting density for angles of incidence $\alpha_i = 0.2°$ and $\alpha_i = 1.0°$ and Q_{GINSES}=0.06 Å^{-1}. Solid lines are fits of eq 14 to the data.

The obtained fitting parameters and corresponding dynamic correlation lengths are displayed in Table 5.

Table 5: GINSES fit parameters.

Sample	α_i	A	A_{bgr}	Γ_i (ns^{-1})	Γ_c (ns^{-1})	ξ_{coop} (nm)
PNIPAM-B-0-120	0.2°	0.60 ± 0.01	0.45 ± 0.03	-	0.019 ± 0.01	2.79
PNIPAM-B-0-120	1.0°	0.72 ± 0.01	0.45 ± 0.04	-	0.010 ± 0.01	5.17
PNIPAM-B-0.2-240	0.27°	0.67 ± 0.01	0.48 ± 0.03	1.6 ± 0.4	0.0083 ± 0.002	6.36
PNIPAM-B-0.2-240	0.5°	0.78 ± 0.01	0.41 ± 0.06	-	0.0034 ± 0.001	15.60
PNIPAM-B-0.2-240	1.3°	0.80 ± 0.01	0.46 ± 0.13	-	0.0021 ± 0.001	25.54

Figures 8 and 9 show the intermediate scattering functions (ISF) S(Q, τ_{NSE}) of both brush samples, PNIPAM-B-0-120 and PNIPAM-B-0.2-240. Solid lines are fits of eqs 14 and 15 to the data.

The results show an increase in the dynamic correlation length ξ_{coop} with an increasing distance from the grafting surface. The brush with the lowest grafting density displays higher values for ξ_{coop} (approximately 2.5 times the value of PNIPAM-B-0-120 at the interface and 5x into the bulk phase). This is in agreement with the expectations, since a lower grafting density means more distance between neighboring polymer chains and therefore more room for chain motion. The findings are also in agreement with theoretical considerations and

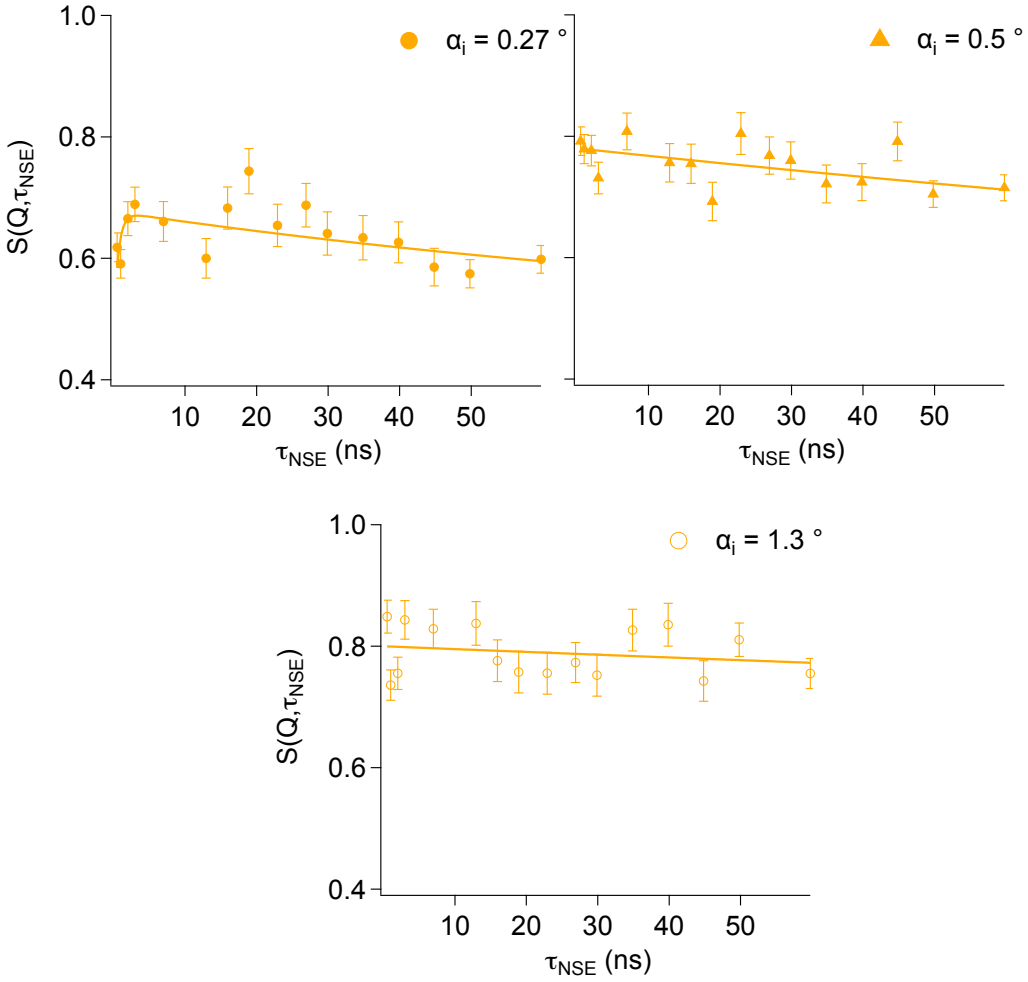

Figure 9: Intermediate scattering functions S(Q, τ_{NSE}) of PNIPAM-B-0.2-240 (low grafting density) for angles of incidence $\alpha_i = 0.27°$, $\alpha_i = 0.5°$ and $\alpha_i = 1.3°$ and Q_{GINSES}=0.06 Å^{-1}. At $\alpha_i = 0.27°$ data was fitted according to eq 15, while all remaining intermediate scattering functions were fitted according to eq 14.

computer simulations by Binder, who describes a non-uniform blob model in which the last blob is considerably bigger than the blobs closer to the grafting surface and can reach up to 10-20% of the entire brush height.[18,49] Results by Binder are also in agreement with the smooth transition between the polymer and solvent phases in the scattering length density profiles obtained from out NR measurements.

The intermediate scattering function $S(Q, \tau_{NSE})$ of the semidilute brush PNIPAM-B-0.2-240 features an initial incline at low Fourier times. This incline is attributed to an incoherent contribution to the scattering signal, which can be fitted using eq 15. The resulting diffusion coefficient shows a value of 4×10^{-9} m^2/s. This corresponds well to the values found for the self-diffusion of first-shell water molecules surrounding PNIPAM in a simulation study by Longhi et al.[50] It can therefore be speculated that the incoherent contribution can be assigned to hydrogen bonds between PNIPAM side chains and protonated water molecules, which is more prevalent at lower grafting densities as a bigger fraction of polymer is found in the vicinity of the grafting surface (compare NR data). However, further experiments would be necessary to gain a better understanding of the source of this incoherent contribution at low Fourier times, which is not the focus of this study.

In a small angle neutron scattering (SANS) measurement we found a correlation length of 2.4 nm for a semidilute PNIPAM solution (c = 0.05 g/mL) with a comparable molar mass of M_n = 30000 g/mol in D_2O at 15 °C.[51] This is in agreement with the values of ξ_{coop} close to the substrate at the smallest neutron penetration depth. This indicates that the investigated PNIPAM brushes have the dynamic signature of a semidilute solution, even when strongly stretched in the high grafting density regime and at large chain lengths as used in our experiments.

Compared to the value found in solution, the correlation length ξ_{coop} is larger at increasing distance from the grafting surface. This suggests that the dense regime is left and the large fluctuations of the chains contribute to the signal. The large values of ξ_{coop} compare to the radius of the swollen chain in good solvent $R_F = 8-11$ nm at the investigated chain lengths

rather than the value of ξ of the semidilute solution.

The small relaxation rates Γ_c (corresponding to large relaxation time) may also result from the hindrance of the diving of the ends into the brush. This could lead to long residence times of the chain ends in the distant region of the brush. In combination with the smoothly decreasing polymer volume fraction profiles $\Phi(z)$ this might result in the measured dynamic signature. It would indicate a stiffening of the brush as predicted by theory.[27] GINSES measurements as described here for polymer brushes of different grafting densities can complement the static structural information usually obtained from ellipsometry and neutron reflectometry. Considering the near surface dynamics at decreasing grafting density may reveal the influence of the solid substrate on the chain mobility which seems to be reduced in case of PNIPAM brushes possibly due to increasing attractive interactions between the tethered polymer chains and the solid substrate.

Conclusion

In this work, the structure and dynamics of PNIPAM brushes grafted from a solid planar substrate under good solvent conditions were probed in the semidilute and concentrated brush regime. The molar mass and molar mass distribution were determined by degrafting of the polymer chains and subsequent size exclusion chromatography. This data was then used to calculate the grafting density and molecular dispersity index of the polymer brush. PNIPAM brushes were prepared by surface initiated atom transfer radical polymerization to achieve high grafting densities at the cost of a higher molecular dispersity. Ellipsometry and neutron reflectometry were employed to probe the brush structure, while neutron spin echo spectroscopy under grazing incidence in reflection mode was used to investigate brush dynamics. A PNIPAM brush in the semidilute regime displayed two distinctive polymer layers with varying polymer volume fractions, where the layer in proximity to the grafting interface was denser in polymer than the one approaching the solvent phase. The concentrated PNIPAM brush displayed only one layer with a smooth transition into the solvent phase.

GINSES studies were carried out on the basis of a recent feasibility study for PEG based brushes by Wellert et al.[12] The number of publications on GINSES and more specifically of GINSES on polymer brushes is still limited, making this work a valuable contribution in further supporting the feasibility argument for these experiments. Furthermore, we simulated the evanescent wave in total reflection geometry with the Distorted Wave Born Approximation with the BornAgain software for a brush and the background sample. These simulations allow to estimate the contributions of brushes and the background to the detected signal. PNIPAM brush dynamics are discussed at different neutron penetration depths (8 nm $\geq$ $z_{1/e}$ $\geq$ 39 μm). The cooperative correlation lengths determined from GINSES are in agreement with non uniform blob theory as the correlation length increases with increasing distance from the grafting interface.

Incoherent scattering contributions in the semidilute regime in vicinity to the grafting interface are explained by contributions from first shell protonated water molecules bound to the PNIPAM brush via hydrogen bonds. However, this contribution has a negligible effect on the results obtained from the coherent scattering signal. It is speculated that an exchange with deuterated water within the denser layers close to the grafting interface is more hindered compared to the outer layer and therefore these contributions are observed only at low neutron penetration depths.

In general, it was shown that GINSES experiments are feasible on PNIPAM brushes of varying grafting densities. However, an improvement of the intensity of the scattering signal is desirable. Also at intermediate neutron penetration depths the resolution in z-direction is still challenging due to the rather broad wavelength distribution of 20%. For future experiments further investigation of the source of the incoherent scattering distribution to the the scattering signal in GINSES experiments is planned.

Acknowledgement

The authors thank Regine von Klitzing for the provision of laboratory equipment for polymer brush syntheses. We also thank Marlies Gräwert for the measurement of SEC chromatograms. This work is based upon experiments performed at the MARIA: Magnetic reflectometer with high incident angle and J-NSE instrument operated by JCNS at Heinz Maier-Leibnitz Zentrum (MLZ), Garching, Germany. Furthermore, we thank Deutsche Forschungsgemeinschaft DFG for funding (grant number WE5066/3-1 (S. Wellert) and HO5488/2-1 (O. Holderer)).

Supporting Information Available

The following files are available free of charge.

- SIWitteMacromolecules2019: Supplementary figures.

References

(1) Milner, S. Polymer Brushes. *Science* **1991**, *251*, 905–914.

(2) Stuart, M. A. C.; Huck, W. T.; Genzer, J.; Müller, M.; Ober, C.; Stamm, M.; Sukhorukov, G. B.; Szleifer, I.; Tsukruk, V. V.; Urban, M.; Winnik, F.; Zauscher, S.; Luzinov, I.; Minko, S. Emerging applications of stimuli-responsive polymer materials. *Nature Materials* **2010**, *9*, 101–113.

(3) Azzaroni, O. Polymer Brushes Here, There, and Everywhere: Recent Advances in Their Practical Applications and Emerging Opportunities in Multiple Research Fields. *Journal of Polymer Science Part A: Polymer Chemistry* **2012**, *50*, 3225–3258.

(4) Senaratne, W.; Andruzzi, L.; Ober, C. K. Self-Assembled Monolayers and Polymer

Brushes in Biotechnology: Current Applications and Future Perspectives. *Biomacromolecules* **2005**, *6*, 2427–2448.

(5) Farago, B.; Monkenbusch, M.; Richter, D.; Huang, J. S.; Fetters, L. J.; Gast, A. P. Collective dynamics of tethered chains: breathing modes. *Physical Review Letters* **1993**, *71*, 1015–1018.

(6) Sigel, R. Light scattering near and from interfaces using evanescent wave and ellipsometric light scattering. *Current Opinion in Colloid & Interface Science* **2009**, *14*, 426–437.

(7) Fytas, G.; Anastadiadis, S. H.; Seghrouchni, R.; Vlassopoulos, D.; Li, J.; Factor, B. J.; Thoebald, W.; Toprakcioglu, C. Probing Collective Motions of Terminally Anchored Polymers. *Science* **1996**, *274*, 2041–2044.

(8) Yu, Y.; Kieviet, B. D.; Liu, F.; Siretanu, I.; Kutnyánszky, E.; Vansco, G. J.; de Beer, S. Stretching of collapsed polymers causes an enhanced dissipative response of PNIPAM brushes near their LCST. *Soft Matter* **2015**, *11*, 8505–8516.

(9) Malham, I. B.; Bureau, L. Density Effects on Collapse, Compression, and Adhesion of Thermoresponsive Polymer Brushes. *Langmuir* **2010**, *26*, 4762–4768.

(10) Roters, A.; Gelbert, M.; Schimmel, M.; Rühe, J.; Johannsmann, D. Static and dynamic profiles of tethered polymer layers probed by analyzing the noise of an atomic force microscope. *Physical Review E* **1997**, *56*, 3256–3264.

(11) Roters, A.; Johannsmann, D. Distance-dependent noise measurements in scanning force microscopy. *Journal of Physics: Condensed Matter* **1996**, *8*, 7561–7577.

(12) Wellert, S.; Hübner, J.; Boyaciyan, D.; Ivanova, O.; von Klitzing, R.; Soltwedel, O.; Holderer, O. A grazing incidence neutron spin echo study of near surface dynamics in

p(MeO_2MA-*co*-OEGMA) copolymer brushes. *Colloid and Polymer Science* **2018**, *296*, 2005–2014.

(13) Gawlitza, K.; Ivanova, O.; Radulescu, A.; Holderer, O.; von Klitzing, R.; Wellert, S. Bulk phase and surface dynamics of PEG microgel particles. *Macromolecules* **2015**, *48*, 5807–5815.

(14) Milner, S. T.; Witten, T. A.; Cates, M. E. Theory of the Grafted Polymer Brush. *Macromolecules* **1988**, *21*, 2610–2619.

(15) de Vos, W. M.; Leermakers, F. A. M. Modeling the structure of a polydisperse polymer brush. *Polymer* **2009**, *50*, 305–316.

(16) Zdyrko, B.; Luzinov, I. Polymer brushes by the "grafting to" method. *Macromolecular Journals* **2011**, *32*, 859–869.

(17) Halperin, A. In *Soft Order in Physical Systems*; Rabin, Y., Bruinsma, R., Eds.; B; Plenum Press: New York, 1994; Vol. 323; Chapter On Polymer Brushes and Blobology: An Introduction, pp 33–56.

(18) Wittmer, J.; Johner, A.; Joanny, F.; Binder, K. Chain desorption from a semidilute polymer brush: A Monte Carlo simulation. *The Journal of Chemical Physics* **1994**, *101*, 4379–4390.

(19) Tsujii, Y.; Ohno, K.; Yamamoto, S.; Goto, A.; Fukuda, T. Structure and Properties of High-Density Polymer Brushes Prepared by Surface-Initiated Living Radical Polymerization. *Advances in Polymer Science* **2006**, *197*, 1–45.

(20) Lai, P.; Binder, K. Structure and dynamics of grafted polymer layers: A Monte Carlo simulation. *Journal of Chemical Physics* **1991**, *95*, 9288–9299.

(21) Raphael, E.; Pincus, P.; Fredrickson, G. H. Conformation of Star Polymers in High Molecular Weight Solvents. *Macromolecules* **1993**, *26*, 1996–2006.

(22) Coluzza, I.; Hansen, J. Transition from Highly to Fully Stretched Polymer Brushes in Good Solvent. *Physical Review Letters* **2008**, *100*, 016104.

(23) Binder, K.; Milchev, A. Polymer Brushes on Flat and Curved Surfaces: How Computer Simulations Can Help to Test Theories and to Interpret Experiments. *Journal of Polymer Science, Part B: Polymer Physics* **2012**, *50*, 1515–1555.

(24) Klok, H.; Genzer, J. Expanding the Polymer Mechanochemistry Toolbox through Surface-Initiated Polymerization. *ACS Macro Letters* **2015**, *4*, 636–639.

(25) Paripovic, D.; Klok, H. Improving the Stability in Aqueous Media of Polymer Brushes Grafted from Silicon Oxide Substrates by Surface-Initiated Atom Transfer Radical Polymerization. *Macromolecular Chemistry and Physics* **2011**, *212*, 950–958.

(26) de Gennes, P. G. Polymers at an interface; a simplified view. *Advances in Colloid and Interface Science* **1987**, *27*, 189–209.

(27) He, G.; Merlitz, H.; Sommer, J.; Wu, C. Static and Dynamic Properties of Polymer Brushes at Moderate and High Grafting Densities: A Molecular Dynamics Study. *Macromolecules* **2007**, *40*, 6721–6730.

(28) Klein, J. Structure and Dynamics of Polymer Chains Tethered at the Solid-Liquid Interface. *Journal of Macromolecular Science, Part A Pure and Applied Chemistry* **1992**, *29*, 99–106.

(29) Christau, S.; Möller, T.; Genzer, J.; Koehler, R.; von Klitzing, R. Salt-Induced aggregation of negatively charged gold nanoparticles confined in a polymer brush matrix. *Macromolecules* **2017**, *50*, 7333–7343.

(30) Boyaciyan, D.; Krause, P.; von Klitzing, R. Making strong polyelectrolyte brushes pH-sensitive by incorporating of gold nanoparticles. *Soft Matter* **2018**, *14*, 4029–4039.

(31) Christau, S.; Möller, T.; Yenice, Z.; Genzer, J.; von Klitzing, R. Brush/gold nanoparticle hybrids: effect of grafting density on the particle uptake and distribution within weak polyelectrolyte brushes. *Langmuir* **2014**, *30*, 13033–13041.

(32) Yim, H.; Kent, M.; Mendez, S.; Lopez, G.; Satija, S.; Seo, Y. Effects of grafting density and molecular weight on the temperature-dependent conformational change of poly (*N*-isopropylacrylamide) grafted chains in water. *Macromolecules* **2006**, *39*, 3420–3426.

(33) Patil, R. R.; Turgman-Cohen, S.; Srogl, J.; Kiserow, D.; Genzer, J. On-demand degrafting and the study of molecular weight and grafting density of poly(methyl methacrylate) brushes on flat silica substrates. *Langmuir* **2015**, *31*, 2372–2381.

(34) Mattauch, S. et al. The high-intensity reflectometer of the Jülich Centre for Neutron Science: MARIA. *Journal of Applied Crystallography* **2018**, *51*, 6.

(35) Brouette, N.; Xue, C.; Haertlein, M.; Moulin, M.; Fragneto, G.; Leckband, D. E.; Halperin, A.; Sferrazza, M. Protein adsorption properties of OEG monolayers and dense PNIPAM brushes probed by neutron reflectivity. *The European Physical Journal Special Topics* **2012**, *213*, 343–353.

(36) Pasini, S.; Holderer, O.; Kozielewski, T.; Richter, D.; Monkenbusch, M. J-NSE-Phoenix, a neutron spin-echo spectrometer with optimized superconducting precession coils at the MLZ in Garching. *Review of Scientific Instruments* **2019**, *90*, 043107.

(37) Nouhi, S.; Hellsing, M. S.; Kapaklis, V.; Rennie, A. R. Grazing-incidence small-angle neutron scattering from structures below an interface. *Journal of Applied Crystallography* **2017**, *50*, 1066–1074.

(38) Mezei, F., Ed. *Neutron Spin Echo*; Lecture Notes in Physics; Springer-Verlag Berlin Heidelberg: Berlin Heidelberg, 1979; Vol. 128.

(39) Vineyard, G. H. Grazing-incidence diffraction and the distorted-wave approximation for the study of surfaces. *Physical Review B* **1982**, *26*, 4146.

(40) Xiao, D.; Wirth, M. J. Kinetics of surface-initiated atom transfer radical polymerization of acrylamide on silica. *Macromolecules* **2002**, *35*, 2919–2925.

(41) Krys, P.; Matyjaszewski, K. Kinetics of atom transfer radical polymerization. *European Polymer Journal* **2017**, *89*, 4.

(42) Micciulla, S.; Michalowsky, J.; Schroer, M. A.; Holm, C.; von Klitzing, R.; Smiatek, J. Concentration dependent effects of urea binding to poly (*N*-isopropylacrylamide) brushes: a combined experimental and numerical study. *Physical Chemistry Chemical Physics* **2016**, *18*, 5324–5335.

(43) Kooij, E. S.; Sui, X.; Hempenius, M. A.; Zandvliet, H. J.; Vancso, G. J. Probing the thermal collapse of poly (*N*-isopropylacrylamide) grafts by quantitative in situ ellipsometry. *The Journal of Physical Chemistry B* **2012**, *116*, 9261–9268.

(44) Yu, Y.; M. Cirelli, B. D. K.; Kooij, E. S.; Vansco, G. J.; de Beer, S. Tunable friction by employment of co-non-solvency of PNIPAM brushes. *Polymer* **2016**, *102*, 372–378.

(45) Reufer, M.; Díaz-Leyva, P.; Lynch, I.; Scheffold, F. Temperature-sensitive poly(*N*-isopropylacrylamide) microgel particles: A light scattering study. *The European Physical Journal E* **2009**, *28*, 165–171.

(46) Pasetto, P.; Blas, H.; Audouin, F.; Boissiere, C.; Sanchez, C.; Save, M.; Charleux, B. Mechanistic insight into surface-initiated polymerization of methyl methacrylate and styrene via ATRP from ordered mesoporous silica particles. *Macromolecules* **2009**, *42*, 5983–5995.

(47) Brittain, W. J.; Minko, S. A structural definition of polymer brushes. *Journal of Polymer Science Part A: Polymer Chemistry* **2007**, *45*, 3505–3512.

(48) Descas, R.; Sommer, J.; Blumen, A. Grafted Polymer Chains Interacting with Substrates: Computer Simulations and Scaling. *Macromolecular Theory and Simulations* **2008**, *17*, 429–453.

(49) Binder, K. Scaling concepts for polymer brushes and their test with computer simulation. *The European Physical Journal E* **2002**, *9*, 293–298.

(50) Longhi, G.; Lebon, F.; Abbate, S.; Fornili, S. L. Molecular dynamics simulation of a model oligomer for poly(*N*-isopropylamide) in water. *Chemical Physics Letters* **2004**, *386*, 123–127.

(51) Witte, J.; Kyrey, T.; Lutzki, J.; Dahl, A. M.; Houston, J.; Radulescu, A.; Pipich, V.; Stingaciu, L.; Kühnhammer, M.; Witt, M. U.; von Klitzing, R.; Holderer, O.; Wellert, S. A comparison of the network structure and inner dynamics of homogeneously and heterogeneously crosslinked PNIPAM microgels with high crosslinker content. *Soft Matter* **2019**, *15*, 1053–1064.

Table of Contents Graphic

Grazing Incidence Neutron Spin Echo Study of Poly(*N*-isopropylacrylamide) Brushes

Judith Witte, Patrick Krause, Tetyana Kyrey, Anna Margarethe Dahl, Jana Lutzki, Bernhard V. K. J. Schmidt, Marina Ganeva, Alexandros Koutsioubas, Olaf Holderer, Stefan Wellert

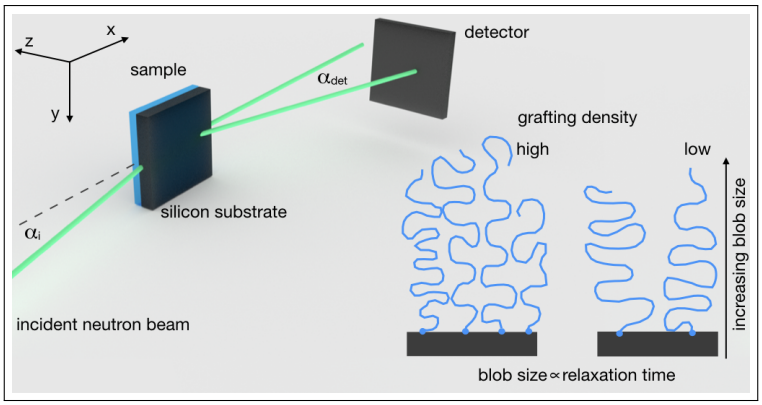

Figure 10: For Table of Contents Use Only